DOI: 10.18727/0722-6691/5335

Scientific Highlights from Ten Years of the MUSE Collaboration

Roland Bacon[1]
Jarle Brinchmann[2]
Nicolas Bouché[1]
Thierry Contini[3]
Sebastian Kamann[4]
Davor Krajnović[5]
Ana Monreal Ibero[6]
Johan Richard[1]
Tanya Urrutia[5]
Lutz Wisotzki[5]
and the MUSE collaboration

[1] Lyon Astrophysics Research Centre, University of Lyon, CNRS, France
[2] Institute of Astrophysics and Space Science, University of Porto, Portugal
[3] Institute for Research in Astrophysics and Planetology, CNRS, University of Toulouse, France
[4] Astrophysics Research Institute, Liverpool John Moores University, UK
[5] Leibniz Institute for Astrophysics, Potsdam, Germany
[6] Leiden Observatory, Leiden University, the Netherlands

We present the scientific highlights of ten years of exploitation of the Multi Unit Spectroscopic Explorer (MUSE) Guaranteed Time Observations performed in the context of the MUSE collaboration. These ten years have been particularly rich in discoveries and have resulted in more than 120 refereed papers. In this article we focus on the main results, grouped into four broad topical categories: resolved stellar populations, nearby galaxies, galaxy demographics, and the circumgalactic medium.

Introduction

About 20 years ago we proposed building the Multi-Unit Spectroscopic Explorer (MUSE) as a second-generation instrument for ESO's Very Large Telescope (VLT). MUSE was conceived to combine the qualities of a sensitive high-resolution imager with those of a powerful integral field spectrograph, capable of not only single-object studies but also opening up the possibility of conducting spectroscopic surveys in deep fields and crowded regions without any target preselection (Bacon et al., 2010). After 10 years of designing, planning, and manufacturing, MUSE was successfully deployed at the VLT's Unit Telescope 4 (UT4) in January 2014 (Bacon et al., 2014) and almost instantly started to produce science-grade data of a hitherto unknown quality (and file sizes). MUSE has now been in regular operation since October 2014 and has become one of the most in-demand ESO instruments. In 2017 and 2018 its performance was further enhanced by the addition of the Adaptive Optics Facility at UT4 (deploying ground layer adaptive optics and laser tomography adaptive optics).

After handing over the keys to ESO we, the MUSE consortium, decided to stay together as a team and exploit our 255 nights of Guaranteed Time Observations (GTO) in a collaborative effort. Ultimately this effort stretched over nearly 10 years — always absorbing only a small fraction of the total time available for MUSE — and was finally concluded (in the sense of recording the very last GTO photons) only a few weeks before finishing this article. Here we take the opportunity to give an overview of the science projects that we focused on within GTO, and to summarise the key accomplishments.

We present these results grouped into four broad topical categories: resolved stellar populations, nearby galaxies, galaxy demographics, and the circumgalactic medium. While each topic encompasses a variety of target types, observing strategies, and detailed science goals, the projects within a category share at least several methodical aspects of the data analysis. Furthermore, the observational data obtained in GTO have often served multiple, sometimes very different, scientific purposes. This is particularly the case for our MUSE surveys in fields with deep Hubble Space Telescope (HST) and multiwavelength data, where we performed 'spectroscopy of everything' down to unprecedented depths. And although this observing strategy was already largely decided before MUSE went on sky, we encountered many surprises, including some of the most influential MUSE discoveries.

Resolved stellar populations

MUSE has been a game-changer in terms of our ability to study stellar populations in the local Universe. By combining precise astrometric information with algorithms to recover the point spread function (PSF), tools like PampelMuse (Kamann, Wisotzki & Roth, 2013) enabled us for the first time to gather large spectroscopic samples even in the crowded environments of massive star clusters or nearby galaxies. This novel approach of 'crowded field spectroscopy' has led to several breakthrough results, as highlighted below.

In a core GTO programme we performed a stellar census of Galactic globular clusters, presented by Kamann et al. (2018).

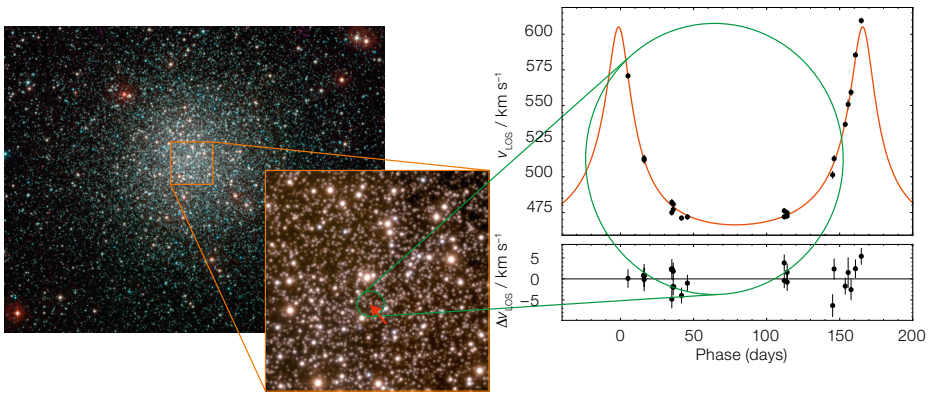

Figure 1. Discovery of a dormant stellar-mass black hole in the Galactic globular cluster NGC 3201. The left panel shows a wide-field image of the cluster taken with the ESO/MPG 2.2-metre telescope at La Silla. Outlined in orange are the contours of a 2 × 2 MUSE mosaic shown in the centre of the Figure. The companion to the stellar-mass black hole is indicated with a red arrow and its phase-folded radial velocity curve is shown to the right. The red line shows the Keplerian motion predicted if the unseen companion is a black hole with a minimum mass of 4.2 $M_{\odot}$.

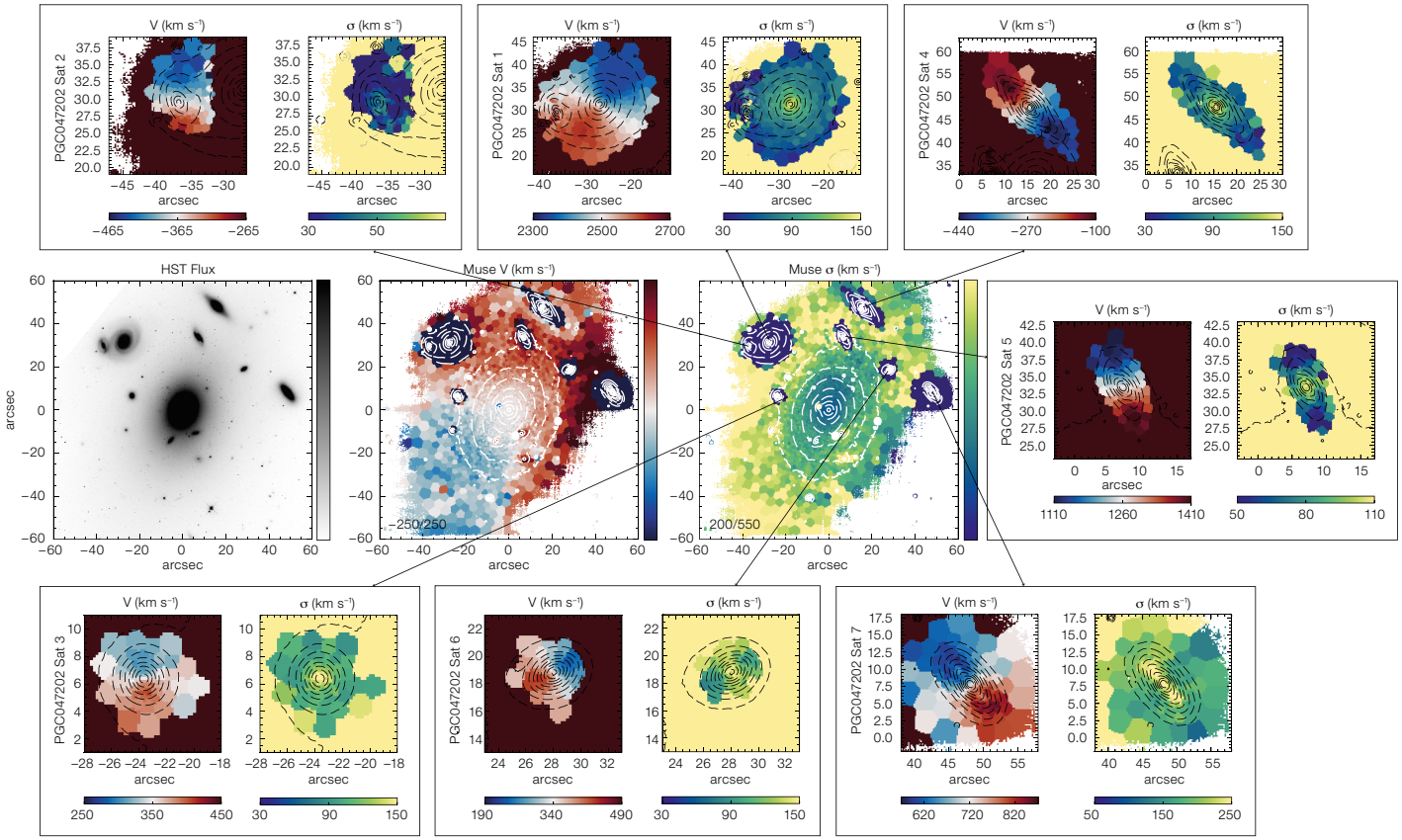

Figure 2. MUSE mosaic of 2 × 2 pointings mapping PGC047202, the BCG in the cluster Abell 3558. The large central panels show the HST/ACS/F814W image, the MUSE mean velocity and the velocity dispersion maps of the stellar component. The velocity limits are given in the lower right corner. The smaller maps show the stellar velocity and velocity dispersion of the satellite galaxies of PGC047202. Their velocities (shown under the maps) are given with respect to the systemic velocity of the main galaxy (set to zero).

For a sample of about 25 clusters we studied the kinematics and chemistry of up to 50 000 cluster stars, and we monitored their radial velocities over eight years in search of variations that would reveal binaries. This campaign led to the detection of a dormant stellar-mass black hole (and two additional candidates) in the globular cluster NGC 3201, presented by Giesers et al. (2018, 2019; see Figure 1). This was not only the first detection of a quiescent black hole in a star cluster, but also the very first dynamical detection of a stellar-mass black hole. It proves that massive star clusters are able to retain sizable black hole populations, which makes them prime candidates to host binary black hole mergers, observable in gravitational waves.

MUSE also allowed us to study the kinematics of globular clusters in unprecedented detail. Kamann et al. (2018) showed that the majority of massive clusters rotate, and that their angular momenta scale with their relaxation times. Star clusters evolving in the tidal fields of their host galaxies will lose angular momentum as stars escape, and the rate of escaping stars is linked to their relaxation times. Therefore, the link between the two suggests that the rotation we observe today is only a fraction of the clusters' natal rotation. In this way MUSE has already improved our understanding of the conditions in which globular clusters — which represent some of the oldest constituents of our Milky Way — formed.

Another relic from the infancy of the Milky Way is the population of ultra-faint dwarf galaxies (UFDs) surrounding it. UFDs are dominated by dark matter and notoriously poor in stars, but are nevertheless challenging to target with multi-object spectrographs because of the low contrast between member stars and surrounding stars and galaxies, and, in some cases, the stellar crowding near their centres. By adopting the crowded field spectroscopy technique we could bypass the challenge of sample pre-selection and efficiently measure radial velocities for faint stars, using their kinematic and dynamical signatures to place constraints on dark matter models. With this goal in mind we carried out MUSE-Faint, a survey of UFDs with MUSE. In the first paper of this survey we used observations of Eridanus 2 to show that the overdensity present in the galaxy is actually a star cluster hosted by this galaxy (Zoutendijk et al., 2020). We then used the existence of this cluster to place constraints on the fraction of dark matter in massive compact halo objects.

Since the UFDs have little baryonic matter, any significant core in the dark matter density profile would present a challenge to the cold dark matter (CDM) model.

Zoutendijk et al. (2021a) carried out the first test of this using data from Eridanus 2 and found that its density profile is consistent with CDM. This work was extended by Zoutendijk (2022) and a forthcoming paper analyses the dark matter density profiles of all five UFDs from Zoutendijk et al. (2021b), providing even stronger constraints on dark matter models.

Located almost an order of magnitude further away than the UFDs at a distance of 1.9 Mpc, the galaxy NGC 300 has been the target of a GTO programme to identify and classify a multitude of discrete objects, again adopting the new approach of crowded field spectroscopy. A pilot study (Roth et al., 2018) revealed several emission line nebulae — H II regions, supernova remnants and planetary nebulae — alongside a large variety of luminous stellar sources such as carbon- and oxygen-rich asymptotic giant branch stars, and symbiotic and other emission-line stars. Hot massive stars are of particular interest for probing the theory of stellar evolution, chemical enrichment and feedback, and as progenitors to black holes. González-Torà et al. (2022) performed quantitative spectroscopy of 16 BA supergiants in a single MUSE pointing and we were able to place these stars into the Hertzsprung–Russell diagram, extending the so-called flux-weighted gravity luminosity relationship to higher surface gravity, and enabling us to obtain a new estimate of the distance modulus of the galaxy, $(m–M)_{FGLR} = 26.34 \pm 0.06$.

Nearby galaxies

We devoted several GTO programmes to the study of galaxies in the nearby Universe, to investigate the role of star formation at different levels and the dynamics of their stellar and gaseous components. Here we use the qualifier ‘nearby’ to denote objects close enough to resolve their inner structures over scales of less than 1 kpc, but already too far away to resolve their contents into individual sources. Within this category, however, the definition of the various samples and the typical properties in these samples vary quite substantially.

At the high end of the distribution of star formation rates, we observed around thirty Luminous and Ultraluminous Infrared Galaxies. A primary target among them was the Antennae system, one of the most iconic galaxies known and the closest (at 22 Mpc) ongoing major merger. We mapped its main body together with the tip of one of the tidal tails at a spatial scale of 100 pc arcsec^{-1}, allowing us to systematically separate H II regions from the diffuse ionised gas (DIG). Combining the measured Hα luminosities with HST photometry of young star clusters we inferred that the dominant ionisation mechanism of the DIG is UV radiation leaking from the main sites of star formation, with escape fractions (from the H II regions, not from the galaxy as a whole) of up to 90%; there is no need for additional sources of ionising photons (Weilbacher et al., 2018). This study was complemented by age-dating the stellar populations in the H II regions in the system (Gunawardhana et al., 2020). A surprising result was the detection of two diffuse interstellar bands, spectral absorption features of mysterious origin, at various locations across the galaxy (Monreal-Ibero, Weilbacher & Wendt, 2018) — the first time that these features had been mapped beyond the Local Group.

We also observed several blue compact dwarf galaxies to probe the impact of extreme star formation on the interstellar medium of galaxies at much lower masses and lower metallicities. An illustrative example is UM 462, a nearby galaxy with properties similar to the so-called green pea galaxies, where we could use the rich information content of a MUSE datacube to disentangle its complex gas structures and the impact of stellar feedback (Monreal-Ibero et al., 2023).

Moving to more typical systems, we mapped a sample of about 40 spiral galaxies on the stellar mass – star formation rate main sequence to investigate the relation of the diffuse interstellar gas to denser gas responsible for star formation. Erroz-Ferrer et al. (2019) showed that these two gas components have different metallicities (star-forming gas being more metal-rich than diffuse gas), but with similar radial variations. Subsequently, den Brok et al. (2020) demonstrated that the star forming gas and the DIG differ in their kinematic properties: while the rotation curves follow a similar trend, the diffuse gas is slower and has higher velocity dispersion. The ‘dynamically hotter’ nature of the DIG was confirmed by dynamical modelling, suggesting that the DIG gas is distributed in a disc-like structure that is considerably thicker than the thin disc holding the star forming gas.

At the other extreme of the range of star formation rates are the quenched systems, i.e. those with little or no star formation activity. Such objects are particularly common among very massive galaxies. As part of our GTO programme we conducted the MUSE Most Massive Galaxies (M3G) survey which targetted some of the most massive galaxies in the nearby Universe. We focused on a sample of Brightest Cluster Galaxies (BCGs) together with a selection of massive ($> 10^{12}\ M_{\odot}$) neighbours, all located in very dense clusters (see Figure 2). While presently not completely devoid of gas (Pagotto et al., 2021), these systems show a high fraction (75–90%) of accreted stars, suggesting an assembly history dominated by merging (Spavone et al., 2021).

The detailed kinematic and dynamical properties revealed by MUSE provide important clues towards understanding which type of mergers were involved in the assembly of these galaxies. Their kinematics is often very complex, with multiple spin reversals and generally low stellar angular momentum. Remarkably, about 50% of BCGs in the sample show evidence of rotation around their major axis (Krajnović et al., 2018), suggested to be the signature outcome of major ‘dry’ (similar mass, gas free) mergers. Such mass assembly pathways are also confirmed by looking at the internal orbital structures: the most massive galaxies are all strongly triaxial systems containing all major orbital families, with co- and counter-rotating spin orientations, resulting in truly spectacular observed kinematics (den Brok et al., 2021).

Galaxy demographics

Among the great scientific successes of the MUSE GTO programme are undoubtedly the MUSE surveys in deep fields, which exploited the multiplexing capability of the instrument in completely new ways. A substantial fraction of our

invested observing time was focused on a systematic spectroscopic mapping of the area in and around the Hubble Ultra Deep Field (HUDF), selected only on the basis that it had the best available multi-band HST coverage to complement the MUSE data (Bacon et al., 2017, 2023; Urrutia et al., 2019). In other fields we took advantage of the presence of strong lensing clusters in the foreground (Bina et al., 2016; Richard et al., 2021). We also surveyed several galaxy groups in the COSMOS area (Epinat et al., 2023).

A key ingredient of our 'spectroscopy of everything' approach adopted for these MUSE deep fields was the development of dedicated software to perform 'blind' searches for emission-line sources. This enabled us to build large samples of objects with extremely faint continuum levels, way below the limit for inclusion in a photometrically selected sample. We are thus probing star-forming galaxies down to extremely low stellar masses. In conjunction with the redshift-dependent survey volume corresponding to a fixed field of view, the two emission lines most frequently selected are [O II] λ3727 and Lyman-α λ1216. The former is detectable with MUSE at (roughly) $0.3 < z < 1.5$, the latter at $2.9 < z < 6.7$. In the following we denote these two redshift intervals as 'intermediate' and 'high' redshifts. In between the two domains there is a region from $z = 1.5$ to 2.9 where galaxies do not show strong emission lines, clearly visible as a 'redshift desert' in the overall redshift distribution (see Figure 3). Here we report on some key results of these deep field surveys, with an emphasis on galaxy demographics and scaling relations.

In the high-redshift range the dominant population studied with MUSE consists of star-forming Lyman-α-emitting galaxies (LAEs), which because of their low stellar masses are far more numerous than the relatively massive 'Lyman-break galaxies' (LBGs). In contrast to narrowband surveys for LAEs or broadband surveys for LBGs, MUSE provides substantial samples of spectroscopically confirmed galaxies in a single observational pass, without any need to preselect targets. Even with a single hour of observing time per pointing, as adopted in the MUSE-Wide survey, we detect typically 11 LAEs in a single MUSE field of 1 arcmin^2 (Herenz et al., 2017). Of course this number increases with exposure time, reaching densities of almost 400 LAEs per arcmin^2 in our deepest dataset encompassing 140 hours — the MXDF (Bacon et al., 2023). Altogether we have already identified several thousand LAEs which we can study in detail.

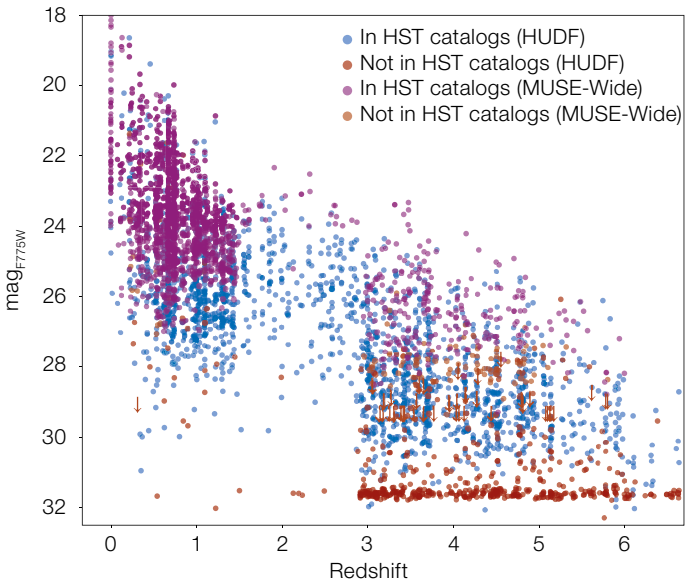

Figure 3. Magnitude–redshift scatter plot for well over 4000 sources in both the HUDF and the surrounding MUSE-Wide fields (adapted from Bacon et al., 2023 and Urrutia et al., 2019). As the shallower MUSE-Wide survey covers a larger volume, more low-redshift sources are spectroscopically identified, while the deeper HUDF data identify more LAEs. Nevertheless, even in the 1-hour data, over 20% of LAEs do not have a catalogued HST counterpart.

One of the most important tools with which to characterise galaxy populations is the luminosity function. For LAEs this quantity is related to the production and escape of H-ionising photons. Getting the correct shape and redshift evolution of the LAE luminosity function, especially at the faint end, is therefore imperative for determining which galaxies dominate the cosmic ionisation budget. One of the challenges that we faced was that the generally very extended nature of Lyman-α emission (see below) impacts the detectability of LAEs. Taking this into account when constructing the survey selection function, we found the faint-end slope of the LAE luminosity function to be considerably steeper than it would have been if we had assumed point sources (Drake et al., 2017; de La Vieuville et al., 2019; Herenz et al., 2019).

Since our blind emission line search technique is not bound to any photometric pre-selection, we are sensitive to finding objects with even extremely high Lyman-α equivalent widths. It turns out that such objects exist in surprisingly large numbers. Almost 20% of the LAEs do not have a counterpart even in the deepest existing HST images, implying very low stellar masses and extreme equivalent widths of > 240 Å (Hashimoto et al., 2017; Maseda et al., 2018; Kerutt et al., 2022). These objects challenge traditional star formation models (for example, Charlot & Fall, 1993; Schaerer, 2002), except for the most extreme stellar populations with low metallicities and a top-heavy initial mass function. In combination with Spitzer infrared photometry to infer Hα luminosities of a subset of these objects, we obtained extremely high H-ionising photon production rates, suggesting that such ultra faint LAEs are a major contributor to the metagalactic UV radiation field (Maseda et al., 2020).

While Lyman-α is usually the most prominent spectral feature in our high-redshift objects, several spectra also show other UV emission and absorption lines. Some of them are valuable for probing the ionisation states of LAEs, the two most prominent being C III] λ1909, a typical tracer for extreme star formation (Maseda et al., 2017) and, intriguingly, He II λ1640, which requires high ionisation parameters to be as strong as observed (Nanayakkara et al., 2019). We have characterised the global UV emission line properties of our high-redshift samples by stacking (Feltre

et al., 2020) and also object-by-object (Schmidt et al., 2021), finding several indications of extreme star formation, young ages and low gas-phase metallicities.

About a third of our blindly detected emission line sources are intermediate-redshift [O II] emitters at $z < 1.5$, for which MUSE also delivers full spectra, often with additional emission lines apart from the detected line. Exploiting the ionised gas kinematics for spatially resolved galaxies, we extended the Tully–Fisher Relation (TFR) to low stellar masses, showing a high scatter around this relation that is due to the frequent presence of dispersion-dominated galaxies in this mass regime (Contini et al., 2016). However, the environment in which galaxies reside does not have a significant impact on the slope or zero-point of the TFR (Abril-Melgarejo et al., 2021; Mercier et al., 2022). Moreover, we found that the regular stellar kinematics of disc galaxies observed in the local Universe was already in place 4–7 Gyr ago and that their gas kinematics traces the gravitational potential of the galaxy, and therefore is not dominated by shocks and turbulent motions even at sub-kpc scales (Guérou et al., 2017; Patricio et al., 2019).

The main sequence of star-forming galaxies in the low-mass regime follows a sub-linear relation with a steeper slope and higher scatter than in the high-mass regime, in agreement with simulations implementing supernova feedback processes in low-mass halos (Boogaard et al., 2018). Mercier et al. (2022) further showed that the main sequence is offset by ~ 0.2 dex in dense environments, suggesting that the star formation activity is reduced by a factor of ~ 1.5 with respect to field galaxies at $z \sim 0.7$.

We further investigated the relationship between the angular momentum of disc galaxies and their stellar masses, also known as the ‘Fall relation’ (FR). Contini et al. (2016) showed that the FR of star-forming galaxies at intermediate redshifts forms a contiguous transition from spirals to ellipticals, according to the dynamical state of the gas. The redshift evolution of the FR is consistent with simulations but the scatter is also a strong function of the dynamical state of the galaxies (Bouché et al., 2021). These results suggest that star-forming galaxies experience a dynamical transformation and lose their angular momentum, i.e., they become dispersion-dominated, before their morphological transformation to passive galaxies.

Thanks to extreme depth of the MXDF we were able to probe the dark matter content in several galaxies within this single field, for the first time in the low-mass regime at these intermediate redshifts (Bouché et al., 2022). Individual rotation curves up to three effective radii show that dark matter fractions are high, typically around 60–95% (see Figure 4), contrary to what has been found in more massive galaxies at higher redshifts.

Circumgalactic medium

As a wide-field integral field unit with exquisite sensitivity, MUSE is a very powerful line imager, and as such it turned out to be a game charger for studies of the circumgalactic medium (CGM), both for mapping it in emission and for studying it with background sources. For these reasons, we dedicated several GTO programmes specifically to improving our understanding of the gas outside galaxies. These programmes targeted quasars, either to use them as background light sources to probe the CGM in absorption and connect the absorption signal with foreground galaxies detected in MUSE (the MUSEQuBES and MEGAFLOW programmes), or to investigate the quasar environments directly. In addition, several of the deep-field observations (including cluster and galaxy group pointings) turned out to provide important new constraints on the CGM — sometimes based on serendipitous discoveries — over a wide range of dark matter halo masses, ranging from small (10^9) to large (10^{14}) halo masses (illustrated in Figure 5). All transverse sizes given in the following refer to physical, not comoving, distances.

Of key importance here is MUSE’s unprecedented sensitivity to low-surface-brightness signals, enabled by the winning combination of high instrument throughput, the advantage of having dispersed data with very low background, and the often very long exposure times. This has facilitated the detection of the CGM in emission in a wide variety of environments, down to a surface brightness of 1×10^{-18} (3×10^{-20}) erg s^{-1} cm^{-2} arcsec^{-2} in exposure times of 1 hr (140 hr).

Our standard cosmological model predicts that the bulk of the baryons in the Universe should reside in a ‘Cosmic Web’ of intergalactic filaments at $z = 3$ which trace the overall mass distribution. By specifically looking at a few overdense regions within the MXDF, the deepest MUSE-GTO field of 140 hours exposure, such filamentary structures have been revealed at very faint levels in Lyman-α emission (Bacon et al., 2021). By itself, UV fluorescence cannot explain the observed emission levels, and one possible

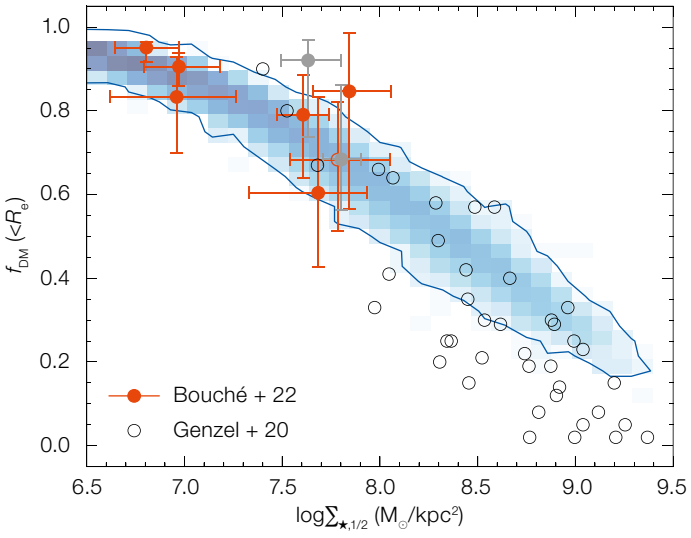

Figure 4. Dark matter fraction (within half-light radius) as a function of stellar mass surface density for nine low-mass star-forming galaxies in the MUSE eXtremely Deep Field. Error bars are 95% confidence intervals, and open circles correspond to the sample of Genzel et al. (2020). The shaded (blue contours) histogram shows the location of $z \sim 1$ central star-forming galaxies in the TNG100 simulations. Adapted from Bouché et al. (2022).

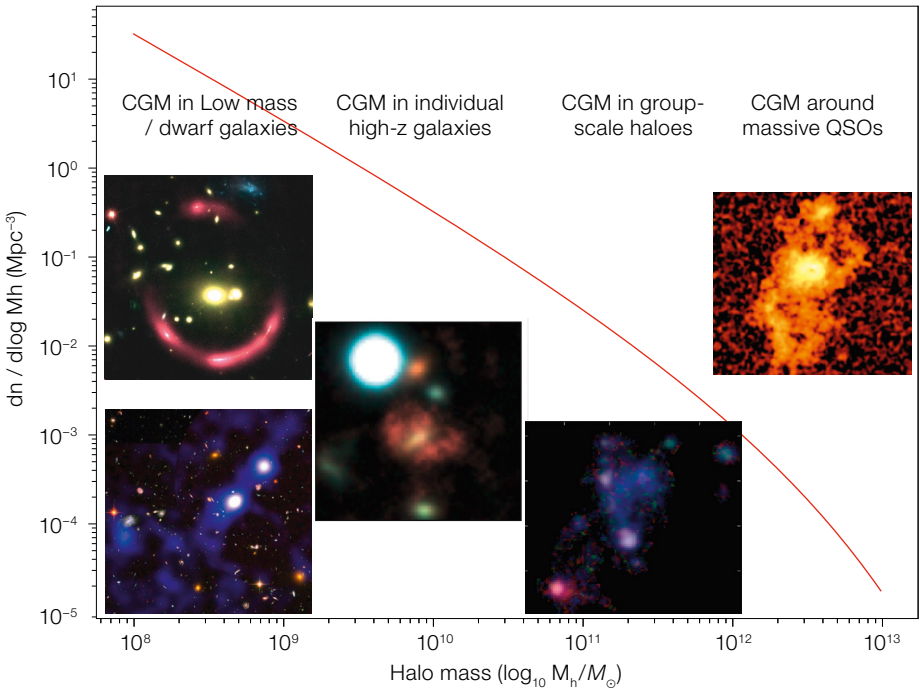

Figure 5. MUSE detections of CGM nebular emission at different mass scales, shown against the halo mass function at z = 3 (red curve). From left to right: extended Lyman-α gas emission around low mass dwarf galaxies found in lensing clusters and ultra-deep fields, anisotropic Mg II emission observed in individual galaxies identified through QSO absorption, diffuse CGM gas found in the intra-group medium, Lyman-α halo surrounding bright QSOs at high redshift.

origin is a very large population of individually undetected 'extreme dwarf' star-forming galaxies with star formation rates per galaxy down to 10^{-4} $M_\odot$ yr^{-1}.

Investigating the Lyman-α emission around 17 quasars at $z \approx 3$, we found very extended structures, sometimes stretching out over more than 100 kpc, in snapshot observations of 1 hr exposure time (Borisova et al., 2016). Remarkably, the detection rate of such Lyman-α quasar nebulae was 100%, very much in contrast to the results of previous (pre-MUSE) surveys using less sensitive instruments. These Lyman-α-bright structures generally have narrow line profiles, and the lack of widespread extended He II and C IV emission suggests that a large fraction of the gas around such massive halos is in the form of cold (T ~ 10^4 K), small (< 20 pc), and metal-poor clumps (Cantalupo et al., 2021).

On the scale of galaxy groups, Leclercq et al. (2022) unveiled extended cold gas shining as Mg II λ2800 emission in a z = 1.31 compact group, distributed over scales of more than 30 kpc, including a low-surface-brightness bridge between two galaxies which suggests that tidal stripping from galaxy interactions is enriching the intragroup medium in the deep MXDF field. At z = 0.7, Epinat et al. (2018) discovered a large gaseous structure in [O II] inside a group in the COSMOS region. The nebula has a radius of more than 150 kpc and contains over 10^{10} $M_\odot$ of ionised gas. We also found several cases of extended ionised gas in massive structures surrounding bright quasars (Johnson et al., 2018, 2022).

On the scale of galaxies ($M_* \approx 10^{10}$ $M_\odot$), Zabl et al. (2021) reported the detection of extended Mg II emission in a deep (11-hr) field around a highly inclined galaxy which happened to be located only 40 kpc from a background quasar observed with high-resolution spectroscopy. The Mg II emission is strongest around the projected minor axis of the galaxy, consistent with gas being ejected from the host by a supernova-driven outflow. A probably related case was noted by Finley et al. (2017) who found evidence for fluorescent Fe II* emission in a galaxy at z = 1.29 which was also aligned with the minor axis.

Around low-mass galaxies ($M_* \approx 10^8$ $M_\odot$), one of the main results from deep MUSE observations is that essentially every Lyman-α-bright high-redshift galaxy shows an extended Lyman-α halo with a characteristic scale ~ 10 times larger than its corresponding stellar continuum emission (Wisotzki et al., 2016; Leclercq et al., 2017). Together with the high spatial density of high redshift galaxies detected, this ubiquity of Lyman-α halos produces an overall background of Lyman-α emission with almost 100% sky coverage (Wisotzki et al., 2018; Kusakabe et al., 2022). When compared to the statistics of Lyman-α absorption against bright background quasars, this result suggests that most circumgalactic atomic hydrogen at these redshifts has now been detected in emission.

Thanks to gravitational lensing by massive galaxy clusters we managed to probe even fainter galaxies and Lyman-α halos, albeit in small volumes. We found that the trends in CGM properties (scale radii, surface brightness profiles) seen in the general (unlensed) deep fields persist down to these low luminosities (Claeyssens et al., 2022). Occasionally the magnification is so strong that the galaxy is stretched out into a giant arc in such a way that we could probe the CGM even at sub-kpc scales, revealing the complexity of its structure in morphological and spectroscopic properties (Claeyssens et al., 2019). One of the most important results was the discovery of significant spatial offsets between the continuum and CGM emission, which possibly indicates the presence of bright star-forming clumps or satellite galaxies surrounding the main CGM halos (Claeyssens et al., 2022).

Using targeted quasar sight-lines with strong metal absorption lines (Mg II with rest-frame equivalent width > 0.5 Å), the MEGAFLOW survey demonstrated that the metals are not distributed isotropically around galaxies (Zabl et al., 2019), but are instead concentrated around the polar and major axis of galaxies out to 60–80 kpc. Furthermore, the metallicity and/or dust content seems enhanced in polar directions (Wendt et al., 2021), consistent with the idea that supernova-driven outflows play a major role in enriching the

CGM. Employing the power of MUSE to find Lyman-α emitters, the MUSEQuBES blind survey of fields around quasars with high-quality spectra of the Lyman-α forest revealed excess H I and C IV absorption near LAEs out to 250 kpc in the transverse direction and 500 km s^{-1} along the line of sight (Muzahid et al., 2021).

Conclusion

The GTO data collection phase is complete, but we still have a long way to go with exploiting the richness of our MUSE data cubes. Analysis is going further for several of the above-mentioned endeavours, and that will keep us busy for some years to come. The astronomical community has also indirectly benefited from our continued involvement in observing with MUSE. We have triggered repeated upgrades of the MUSE Data Reduction System (Weilbacher et al., 2020), and those have played a major role in making MUSE such a popular instrument. We further invested significant effort into developing advanced data analysis software specifically tuned for MUSE science, most of it now in the public domain. We have provided extensive catalogues and user-friendly data access interfaces for several of our deep field surveys and will continue to do so for the remaining fields. Last but not least, all MUSE data including GTO are freely available via the ESO Science Archive Facility. There is undoubtedly still much more science to be conducted with those data, and many discoveries to be made.

References

Abril-Melgarejo, V. et al. 2021, A&A, 647, A152
Bacon, R. et al. 2010, Proc. SPIE, 7735, 773508
Bacon, R. et al. 2014, The Messenger, 157, 13
Bacon, R. et al. 2017, A&A, 608, A1
Bacon, R. et al. 2021, A&A, 647, A107
Bacon, R. et al. 2023, A&A, 670, A4
Bina, D. et al. 2016, A&A, 590, A14
Boogaard, L. A. et al. 2018, A&A, 619, A27
Borisova, E. et al. 2016, ApJ, 831, 39
Bouché, N. F. et al. 2021, A&A, 654, A49
Bouché, N. F. et al. 2022, A&A, 658, A76
den Brok, M. et al. 2020, MNRAS, 491, 4089
den Brok, M. et al. 2021, MNRAS, 508, 4786
Cantalupo, S. et al. 2019, MNRAS, 483, 5188
Charlot, S. & Fall, S. M. 1993, ApJ, 415, 580
Contini, T. et al. 2016, A&A, 591, A49
Drake, A. B. et al. 2017, A&A, 608, A6
Claeyssens, A. et al. 2019, MNRAS, 489, 5022
Claeyssens, A. et al. 2022, A&A, 666, A78
Epinat, B. et al. 2018, A&A, 609, A40
Epinat, B. et al. 2023, submitted to A&A
Erroz-Ferrer, S. et al. 2019, MNRAS, 484, 5009
Feltre, A. et al. 2020, A&A, 641, A118
Finley, H. et al. 2017, A&A, 605, A118
Genzel, R. et al. 2020, ApJ, 902, 98
Giesers, B. et al. 2018, MNRAS, 475, L15
Giesers, B. et al. 2019, A&A, 632, A3
González-Torà, G. et al. 2022, A&A, 658, A117
Guérou, A. et al. 2017, A&A, 608, A5
Gunawardhana, M. L. P. et al. 2020, MNRAS, 497, 3860
Hashimoto, T. et al. 2017, A&A, 608, A10
Herenz, E. C. et al. 2017, A&A, 606, A12
Herenz, E. C. et al. 2019, A&A, 621, A107
Johnson, S. D. et al. 2018, ApJL, 869, L1
Johnson, S. D. et al. 2022, ApJL, 940, L40
Kamann, S., Wisotzki, L. & Roth, M. M. 2013, A&A, 549, A71
Kamann, S. et al. 2018, MNRAS, 473, 5591
Kerutt, J. et al. 2022, A&A, 659, A183
Krajnović, D. et al. 2018, MNRAS, 477, 5327
Kusakabe, H. et al. 2022, A&A, 660, A44
de La Vieuville, G. et al. 2019, A&A, 628, A3
Leclercq, F. et al. 2017, A&A, 608, A8
Leclercq, F. et al. 2022, A&A, 663, A11
Maseda, M. V. et al. 2017, A&A, 608, A4
Maseda, M. V. et al. 2018, ApJL, 865, L1
Maseda, M. V. et al. 2020, MNRAS, 493, 5120
Mercier, W. et al. 2022, A&A, 665, A54
Monreal-Ibero, A., Weilbacher, P. M. & Wendt, M. 2018, A&A, 615, A33
Monreal-Ibero, A. et al. 2023, A&A, 674, A210
Muzahid, S. et al. 2021, MNRAS, 508, 5612
Nanayakkara, T. et al. 2019, A&A, 624, A89
Pagotto, I. et al. 2021, A&A, 649, A63
Patrício, V. et al. 2019, MNRAS, 489, 224
Richard, J. et al. 2021, A&A, 646, A83
Roth, M. M. et al. 2018, A&A, 618, A3
Schaerer, D. 2002, A&A, 382, 28
Schmidt, K. B. et al. 2021, A&A, 654, A80
Spavone, M. et al. 2021, A&A, 649, A161
Urrutia, T. et al. 2019, A&A, 624, A141
Wendt, M. et al. 2021, MNRAS, 502, 3733
Weilbacher, P. M. et al. 2018, A&A, 611, A95
Weilbacher, P. M. et al. 2020, A&A, 641, A28
Wisotzki, L. et al. 2016, A&A, 587, A98
Wisotzki, L. et al. 2018, Nature, 562, 229
Zabl, J. et al. 2019, MNRAS, 485, 1961
Zabl, J. et al. 2021, MNRAS, 507, 4294
Zoutendijk, S. L. et al. 2020, A&A, 635, A107
Zoutendijk, S. L. et al. 2021a, A&A, 651, A80
Zoutendijk, S. L. et al. 2021b, arXiv:2112.09374
Zoutendijk, S. L. 2022, PhD Thesis, Leiden University

A photograph showing most of the telescopes that make up ESO's Very Large Telescope. At the centre, to the right of the setting Sun, Unit Telescope 1 stands ready to observe. It started operating 25 years ago.